The Vacuolar-ATPase Complex Regulates Retinoblast Proliferation and Survival, Photoreceptor Morphogenesis, and Pigmentation in the Zebrafish Eye

Richard J. Nuckels,[1] *Anthony Ng,*[1] *Tristan Darland,*[2] *and Jeffrey M. Gross*[1,3]

Purpose. The vacuolar (v)-ATPase complex is a key regulator of the acidification of endosomes, lysosomes, and the luminal compartments of several cell types, tissues, and organs; however, little is know about the in vivo function of the v-ATPase complex or its roles during eye development. This study was conducted to characterize ocular defects in five zebrafish mutants in which core components of the v-ATPase complex were affected (*atp6v1h*, *atp6v1f*, *atp6v1e1*, *atp6v0c*, and *atp6v0d1*), as well as a sixth mutant in which a v-ATPase associated protein (*atp6ap1*) was affected.

Methods. v-ATPase mutant zebrafish were characterized by histologic, molecular, and ultrastructural analyses.

Results. v-ATPase mutant zebrafish were oculocutaneous albinos and presented with defects in the formation and/or survival of melanosomes and with malformations in the retinal pigmented epithelium (RPE) that compromised melanosome distribution. They were microphthalmic, and BrdU incorporation assays indicated that retinoblast cell cycle exit and sustained proliferation in the ciliary marginal zone (CMZ) were compromised. v-ATPase mutants also possessed elevated levels of apoptotic neurons within their retinas and brains. Photoreceptor outer segment morphology was abnormal in the mutant eye with rosette structures forming adjacent to the affected regions of the RPE. Ultrastructural analyses indicate that RPE cells in v-ATPase mutants possess numerous membrane-bounded vacuoles containing undigested outer segment material. In situ hybridization analyses localized v-ATPase subunit transcripts within the RPE.

Conclusions. These results demonstrate that the v-ATPase complex plays several critical roles during vertebrate eye development and maintenance, and they suggest that defects in v-ATPase complex function could possibly underlie human ocular disorders that affect the RPE. (*Invest Ophthalmol Vis Sci.* 2009;50:893–905) DOI:10.1167/iovs.08-2743

From the [1]Section of Molecular Cell and Developmental Biology and Institute for Cell and Molecular Biology, and the [3]Institute of Neuroscience, The University of Texas at Austin, Austin, Texas; and the [2]Department of Biology, University of North Dakota, Grand Forks, North Dakota.

Supported by Grant M2006-024 from the American Health Assistance Foundation Macular Degeneration Research Program, funds from the Retina Research Foundation and the Karl Kirchgessner Foundation (JMG), and National Institutes of Health Grant K01 DA16291 (TD).

Submitted for publication August 18, 2008; revised September 17, 2008; accepted November 19, 2008.

Disclosure: **R.J. Nuckels**, None; **A. Ng**, None; **T. Darland**, None; and **J.M. Gross**, None

The publication costs of this article were defrayed in part by page charge payment. This article must therefore be marked "*advertisement*" in accordance with 18 U.S.C. §1734 solely to indicate this fact.

Corresponding author: Jeffrey M. Gross, Box C1000, 1 University Station, University of Texas at Austin, Austin, TX 78712; jmgross@mail.utexas.edu.

The retinal pigment epithelium (RPE) serves several critical roles during embryonic eye formation, as well as in maintaining visual function in adults (reviewed in Ref. 1). During development, the RPE is necessary to cue proper development of the adjacent retina and particularly in regulating retinal lamination and photoreceptor morphogenesis (e.g., Refs. 2–4). In adults, RPE cells play a central role in the transport of ions, water, and nutrients between the blood and the retina; the reisomerization of all-*trans*-retinal to 11-*cis*-retinal during the visual cycle; structural support of photoreceptor outer segments; secretion of growth factors and neurotransmitters; and phagocytosis and degradation of shed photoreceptor outer segment debris. Several blinding diseases in humans, such as Leber's congenital amaurosis,[5,6] Best macular dystrophy,[7] and age-related macular degeneration,[8] principally affect the RPE, underscoring its importance in the eye.

Pigmentation of the RPE results from the accumulation of melanin in specialized organelles of RPE cells called melanosomes, which are transported and anchored at the apical surface of RPE cells, such that a uniform black, pigmented layer is apposed to retinal photoreceptors. Melanosomes are mainly specialized in melanin synthesis and storage, but they are also thought to participate in the degradation of phagocytosed photoreceptor outer segments, in conferring protection from oxidative stress, and in the detoxification of visual cycle intermediates.[9–11]

Defects in melanin synthesis or transport result in albinism, which can be subdivided into two general categories: *ocular albinism*, in which solely the eye is affected and *oculocutaneous albinism*, in which the eyes as well as the skin and hair are affected. Albinism is a clinical manifestation in more than 25 genetic disorders in humans, including ocular albinism types I and II, oculocutaneous albinism types I–IV, Hermansky-Pudlak syndrome, Chediak-Higashi syndrome, and Griscelli syndrome.[12–15] Patients with albinism have significantly reduced visual function, with overall acuity ranging from 20/40 to complete blindness.[16] The RPE is severely hypopigmented and underdeveloped in albinism, and these abnormalities cause light scatter and photophobia. Optic nerve projections do not map properly to the lateral geniculate nucleus, leading to strabismus in albinism, and patients also present with macular hypoplasia, which leads to nystagmus.[17,18]

From these and other studies, it is clear that RPE function and proper RPE pigmentation are essential for several aspects of vertebrate eye development and visual function; however, the molecular and cellular processes underlying this requirement remain unclear. With an interest in RPE/retinal interactions and the molecular nature of these interactions, we have examined six recessive zebrafish mutations that present with oculocutaneous albinism and retinal defects.[19,20] The mutations in five of the lines disrupt the loci encoding protein subunits of the vacuolar (v)-ATPase complex (*atp6v0c*, *atp6v0d1*, *atp6v1e1*, *atp6v1h*, and *atp6v1f*), and the sixth mutation disrupts the locus encoding a v-ATPase-associated protein (*atp6ap1*).

v-ATPase is a multiprotein complex, consisting of 13 different subunits assembled into a heteromeric protein complex (Fig. 1[21]). v-ATPases are best known for their roles in proton transport, through which they participate in the acidification of endosomes, lysosomes, and luminal compartments of organs such as the kidney. v-ATPase activity also plays important general roles in regulating protein degradation, intracellular transport, and membrane fusion, and more novel developmental roles in regulating synaptic vesicle exocytosis, patterning of the embryonic left–right axis, and mediating extracellular signaling events by facilitating the release of Hedgehog pathway ligands.[21–26] In addition, a recent study in zebrafish demonstrated that the atp6v0a1 subunit of v-ATPase plays a key role in mediating the fusion between phagosomes and lysosomes in microglia within the brain, and that this fusion is required for neuronal degradation and clearance of apoptotic neurons in vivo.[24]

To date, two human disorders have been attributed to v-ATPase subunit defects: distal renal tubular acidosis and autosomal recessive osteopetrosis, both of which result from homozygosity for mutations in kidney- and bone-specific isoforms of *ATP6V1B1* and *ATP6V0a3*, respectively.[27] No v-ATPase gene mutations have yet been linked to blinding or albinism conditions in humans; however, the v-ATPase complex is expressed on human melanosomes[28] and mouse melanocytes,[29] and v-ATPase subunits are expressed within the zebrafish eye.[30,31]

We present an analysis of the ocular defects in zebrafish v-ATPase mutants. v-ATPase complex function was essential for the cell cycle exit of retinoblasts within the embryonic retina, as well as for the sustained proliferation of retinal stem cells at the ciliary marginal zone (CMZ). v-ATPase function was necessary for the survival of newly generated neurons at the CMZ of the retina, as well as within the ventricular zones of the brain. Finally, our results demonstrated that the v-ATPase complex was essential for patterning and maintenance of photoreceptor outer segments of the retina and for pigmentation and function of the RPE. From these data we conclude that the v-ATPase complex plays a key role in regulating eye growth, neuronal survival and photoreceptor morphogenesis. Given the expression of v-ATPase subunit genes by cells of the RPE, these results suggest that each of the ocular defects observed in v-ATPase mutants might reflect nonautonomous functions for the v-ATPase complex within the RPE.

Materials and Methods

Zebrafish Maintenance and Strains

Zebrafish (*Danio rerio*) were maintained at 28.5°C on a 14-hour light/10-hour dark cycle. Embryos were obtained from the natural spawning of heterozygous carriers set up in pair-wise crosses. Embryos were collected and raised at 28.5°C and were staged according to a method used in a prior study.[32] All animals were treated in accordance with provisions established at the University of Texas at Austin to govern animal use and care and adhered to the ARVO Statement for the Use of Animals in Ophthalmic and Vision Research. Mutant alleles used in the study were *atp6ap1*^{bi112}, *atp6v1h*^{bi923}, *atp6v1f*^{bi1988}, *atp6v1e1*^{bi577a}, *atp6v0d1*^{bi2188b}, and *atp6v0c*^{bi1207}. Because *a82* proved to be allelic to *atp6ap1*, it is referred to as *atp6ap1*^{a82} in agreement with Zebrafish Nomenclature Guidelines.

Reverse-Transcription Polymerase Chain Reaction (RT-PCR)

Ten to 20 embryos were homogenized (TRIzol reagent; Invitrogen, Carlsbad, CA) with a 25-gauge needle and syringe. Total RNA was purified by chloroform extraction and isopropanol precipitation. cDNA from each mutant was synthesized (iScript cDNA synthesis kit; Bio-Rad, Hercules, CA), from 500 ng of total RNA. PCR was performed with 1.25 μL of the resulting cDNA. Primer sequences (shown in Figure 3) were as follows (5′-3′): *atp6ap1*: 5′-1 CTCTGCTCATGCTGCTCATC, 3′-1 TGCACTTGATTTTTCCATGC, 5′-2 CTCCAGCAGAATGACGGAAG, 3′-2 TAGGTGAGGATGAGCAGCAT; *atp6v1e1*: 5′-1 GAGCTGTATTTGCAAAGCAGACGC, V GCTAGCTTGCCAAACCTACAGGT, 3′-1 AGAACCAGTCCGTCCATCAG; *atp6v1b*: 5′-1 AATGCTGAACCGTCAAGACC, 3′-1 CTCCAGCAGGTTCCTGAAAG, 3′-2 CACAACGACAAAAGCACAAGAG; *atp6v0c*: 5′-1 AGCTTTCCTCCCTTTTCTGC, 3′-1 CAGCACCTCTGCAAAGATCA, 5′-2 CCCTTAGTGGACAGGATGAGG; *atp6v1f*: 5′-2 TTGGTGGTGGAGAAGGAAAC, 3′-2 ATCTGCTCAGGCCAGACTGT, 5′-1 TCGCAGTTATCGGTGATGAAG, 3′-1 GCGAGATGGATGAGAATACCC; and *atp6v0d1*: 5′-2 TCAGGCGGATTATTTGAACC, 5′-1 GCTGACGATTATGAGCAGGTC, 3′-2 GAGTGGCGTAGTGCAAGAAAC.

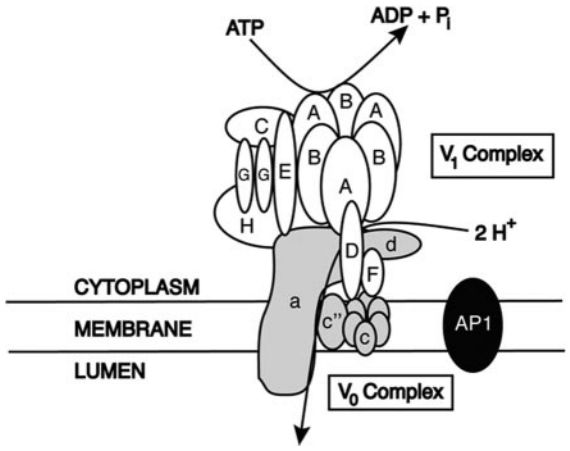

Figure 1. The v-ATPase complex. Schematic of the v-ATPase complex.[21] *Gray*: the V_0 complex components; *white*: V_1 components. atp6ap1 is a v-ATPase-associated protein; however, the nature of its interactions with the complex are unknown. ATP is hydrolyzed by the V_1 complex, which provides energy for two protons to be transported through the membrane V_0 pore into the luminal compartments of organs and/or intracellular organelles.

Histology

Histology was performed as described elsewhere.[33] Briefly, mutant and wild-type sibling embryos were collected and fixed overnight at 4°C in a solution of 1% (wt/vol) paraformaldehyde, 2.5% glutaraldehyde, and 3% sucrose in PBS. They were washed three times for 5 minutes in PBS and refixed for 90 minutes at 4°C in a 1% OsO_4 solution, washed three times for 5 minutes each in PBS at RT, and dehydrated through a graded ethanol series (50, 70, 80, 90, 2 × 100%). Embryos were further dehydrated two times for 10 minutes each in propylene oxide and infiltrated for 1 to 2 hours into a 50% propylene oxide/50% Epon/Araldite mixture (Polysciences, Inc., Warrington, PA). Embryos were then incubated overnight at RT in 100% Epon/Araldite resin with caps open to allow for propylene oxide evaporation and resin infiltration, embedded, and baked at 60°C for 2 to 3 days. Sections (1.5 μm) were cut, mounted on glass slides, and stained in a 1% methylene blue/1% borax solution. Sections were mounted in DPX (Electron Microscopy Sciences, Hatfield, PA) and photographed on a microscope (DMRB; Leica, Deerfield, IL) mounted with a digital camera (DFC320; Leica). Images were subsequently processed with image-management software (CS2 Photoshop; Adobe Systems, San Jose, CA).

Transmission Electron Microscopy

For transmission electron microscopy, embryos were processed for histology, and transverse sections, 70 to 90 nm in thickness, were cut through the central retina and mounted onto grids. The sections were stained with lead citrate and uranyl acetate. The images were obtained on a transmission electron microscope (80 kV, model 208; Philips,

Eindhoven, The Netherlands) via a digital camera (Advantage HR 1MB; AMT Imaging, Danvers, MA) and processed (Photoshop CS2; Adobe Systems).

Riboprobes and In Situ Hybridization

Hybridizations were performed essentially as described by Jowett and Lettice,[34] with digoxigenin labeled antisense RNA probes. cDNA clones containing v-ATPase subunit genes were either purchased from Open Biosystems (Huntsville, AL; *atp6ap1*, *atp6v0d1*, *atp6v1e1*, *atp6v1h*, *atp6v1f*), or cloned from 24-hour post fertilization (hpf) cDNA (*atp6v0c*; cloning details available on request).

Immunohistochemistry

Immunohistochemistry was performed as according to a published method.[35] Briefly, mutants and wild-type siblings were collected and fixed overnight at 4°C in a solution of 4% paraformaldehyde in PBS. The embryos were washed at room temperature (RT) three times for 5 minutes in PBS and then infiltrated with 35% sucrose for 1 to 2 hours at RT. The embryos were then arranged and embedded in plastic molds containing TBS cryopreservation medium (Triangle Biomedical Sciences, Durham, NC). Cryosections 12 μm in thickness were cut on a cryostat (HM550; Microm International, Walldorf, Germany) and attached to gelatin-coated slides. After drying for 1 to 2 hours at RT, the slides were marked with a hydrophobic marker (PAP pen), rehydrated briefly in PBS, and blocked for 1 to 2 hours in 5% NGS. Primary antibodies, diluted in 5% NGS, were added and the slides incubated overnight at 4°C. Slides were then washed in PBS at RT two times for 5 minutes and one time for 30 minutes each and incubated in secondary antibody, diluted in 5% NGS, for 90 minutes at RT. The slides were briefly washed in PBS and the nuclei stained with Sytox Green (1: 10,000; Invitrogen-Molecular Probes, Eugene, OR) for 12 minutes at RT. The slides were then washed three times for 15 minutes in PBS at RT and mounted in antifade mounting medium (Vectashield; Vector Laboratories, Inc., Burlingame, CA). The following antibodies and dilutions were used: 1d1 (1:100), 5e11 (1:100), zpr1 (1:200), zn8 (1: 100), PKC (1:150), and goat anti-mouse Cy3 secondary (1:500). Imaging was performed in a Pascal laser scanning confocal microscope (LSM5; Carl Zeiss Meditec, Inc., Dublin, CA). Three to five optical sections (1 μm in thickness) were collected and projected by using the confocal microscope's software (Carl Zeiss Meditec, Inc.).

BrdU Assays

BrdU incorporation assays were performed as described in Lee et al.[36] Briefly, embryos were dechorionated and exposed to a 10-mM solution of BrdU (Sigma) for defined periods of time and either immediately fixed and processed for immunohistochemistry or washed five times in fresh fish water and cultured until fixation. Cryosectioning and immunohistochemistry were performed as just described, with the addition of a 10-minute incubation at 37°C in 4 M HCl before blocking, to relax the chromatin and facilitate BrdU detection. Rat anti-BrdU (Roche Molecular Diagnostics, Indianapolis, IN) was used at 1:100 in conjunction with a goat anti-rat Cy3 secondary antibody (1:500). Cell counts were performed on sections through the central retina, as indicated by the presence of an optic nerve. BrdU-positive nuclei were identified by their intense fluorescence and were counted from sections obtained from at least three different wild-type or mutant embryos, derived from at least two different mating pairs. Averages of BrdU-positive cells at each time point were compared to wild-type controls by using a Student's *t*-test for statistical significance (Prism; GraphPad Software, San Diego, CA).

TUNEL Assays

TUNEL assays were performed on cryosections with a TMR-red label (In situ Cell Death Detection Kit; Roche Applied Science) per the manufacturer's instructions and were imaged by confocal microscopy.

Results

Zebrafish v-ATPase Mutants

The zebrafish v-ATPase mutant phenotype is characterized by oculocutaneous albinism (Fig. 2). Recessive mutants have reduced pigmentation along their body axis and reduced pigmentation of the RPE. Mutants can be easily distinguished from their wild-type siblings as early as 2 days post fertilization (dpf) as a result of these pigmentation defects (Fig. 4, and data not shown). In the RPE, pigmentation levels varied between mutants with the most severely affected mutants, *atp6v1h*, *atp6v1f*, and *atp6v0c*, showing large patches of nonpigmented RPE in the midst of pigmented RPE (Figs. 2C′, 2D′, 2G′), and the least severely affected mutant, *atp6v1e1*, having near-normal RPE pigmentation (Fig. 2E′). Mutants were microphthalmic with eye sizes ~ 20% smaller on average than their wild-type siblings at 5 dpf, and by external examination, the RPE was morphologically abnormal in some of them (e.g., *atp6v0c*, Fig. 2G). Melanocytes along the body axis were enlarged and abnormal in shape, and they were fainter in their level of black color, likely reflecting a defect in the level and/or distribution of melanin pigment within these cells (Figs. 2H–K). Mutants were also generally smaller then their wild-type siblings and, other than a small number of *atp6ap1* and *atp6v0d1* embryos, most did not inflate their swim bladders. Whereas all organs appeared to be present in the mutants, overt defects in internal organ appearance were detected in some embryos (e.g., brown color of the gastrointestinal tract in *atp6ap1*), and several of the mutants typically presented with larger amounts of unconsumed yolk than did their wild-type siblings (e.g., *atp6v1f*, *atp6v0c*). *atp6v0c* mutants frequently presented with several additional nonocular and/or pleiotropic phenotypes between 5 and 6 dpf. These included pericardial edema, periocular and subdermal swelling, widespread necrosis, and yolk degeneration. *atp6v0c* mutants also showed substantially higher levels of lethality, with most mutants dying by 6 dpf. Beyond these overt analyses, other organ systems have not yet been analyzed in depth, and thus it is entirely possible that they are also affected in the mutants.

Because these mutants were generated through retroviral insertional mutagenesis[19,37] we first wanted to determine what effect that proviral insertion had on expression of the locus. In Figure 3, the approximate position of each proviral insertion has been mapped onto a schematic of the mutated gene (www.ensembl.org/Danio_rerio/[38]). RT-PCR was then performed on total RNA samples isolated from 5 dpf wild-type and mutant embryos from each line, and transcript levels were assayed for each v-ATPase subunit using primer sets flanking and/or downstream of the proviral insert (Fig. 3). Transcripts from the mutated locus were undetectable in two of the mutants, *atp6v1h* (Fig. 3B) and *atp6v0c* (Fig. 3F), and transcript levels were dramatically reduced in two others, *atp6ap1* (Fig. 3A) and *atp6v1f* (Fig. 3C). In *atp6v1e1* mutants, the proviral insert was located in the 5′UTR, and it was transcribed into an abnormal N-terminal fragment mRNA (Fig. 3D). With the large proviral insertion included in the 5′UTR, it is doubtful that this aberrant *atp6v1e1* transcript would be efficiently translated into protein, and it is likely to be degraded in most embryos. In *atp6v0d1* mutants, the proviral insertion is located in the sixth intron of the *atp6v0d1* gene, which results in mRNA splicing defects in which a portion of the viral sequence is spliced into a subset of *atp6v0d1* transcripts (Fig. 3E). Sequencing these splice variants revealed a frameshift in the *atp6v0d1* coding sequence, which leads to the translation and inclusion of a portion of the viral sequence into the atp6v0d1 protein and generates a premature stop codon (*data not shown*). The net result of this is truncation of the atp6v0d1 protein and an

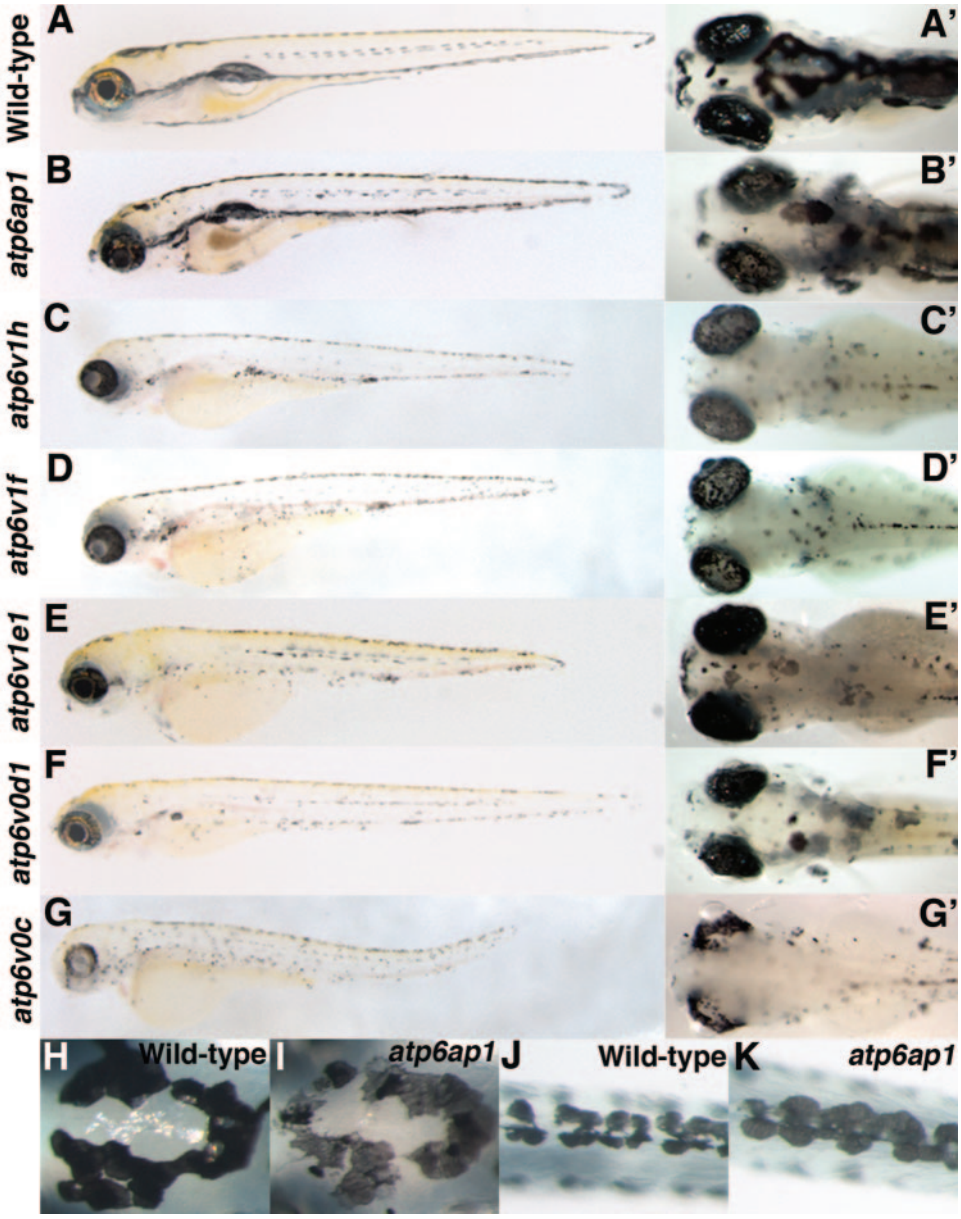

FIGURE 2. Zebrafish v-ATPase mutants. v-ATPase mutants present with various degrees of oculocutaneous albinism and microphthalmia. Shown are lateral views of 5-dpf wild-type (**A**), *atp6ap1* (**B**), *atp6v1h* (**C**), *atp6v1f* (**D**), *atp6v1e1* (**E**), *atp6v0d1* (**F**), and *atp6v0c* (**G**) mutants, and higher magnification dorsal views (**A′**–**G′**). In the RPE, pigmentation defects ranged from slight hypopigmentation (*atp6v1e1*) to severe hypopigmentation (*atp6v1h*), when compared with a wild-type embryos. Melanophore shape and distribution along the body axis were also affected in each of the mutants. (**H**, **I**) dorsal head; (**J**, **K**) dorsal tail.

absence of the 53 terminal amino acids encoded by exons 7 and 8.

From the results of these RT-PCR assays, we conclude that the *atp6ap1*, *atp6v1h*, *atp6v0c*, *atp6v1f*, and *atp6v1e1* mutations are null alleles. Given the similarity in phenotypes between the different v-ATPase subunit mutations, we also predict that the *atp6v0d1* mutation is a null allele, but we cannot rule out the possibility that it encodes a protein with dominant-negative activity. No embryonic phenotype was observed in *atp6v0d1* heterozygotes, suggesting that this is not likely to be the case; however, no structure–function studies have been reported for the v0d subunit that would inform us as to the function of these 53 C-terminal residues.[39]

Histologic Analysis of the v-ATPase Mutant Eye

Our previous studies have shown that v-ATPase mutants are unresponsive to visual stimuli in optokinetic response assays and that this probably results from underlying defects in retinal and/or RPE development.[20] To better assess the visual system defects in v-ATPase mutants, we first performed a series of histologic analyses over the first 5 days of embryonic development to identify the full scope of the v-ATPase mutant ocular phenotype.

The wild-type eye at 2 dpf contained a well-formed lens and a thin but well-pigmented RPE, and retinal lamination had commenced in the central retina with an obvious ganglion cell layer (GCL) and inner plexiform layer (IPL) present at this point (Fig. 4A). Proliferation continued at the retinal periphery in the CMZ (Fig. 4A). v-ATPase mutants could be identified at 2 dpf, and by comparison to the wild-type at this time, the v-ATPase mutant eye possessed a thinner and less-pigmented RPE (Figs. 4B–G). Lens development was normal but retinal lamination was slightly delayed relative to that in the wild-type eye. Overall eye size was also smaller, and therefore the mutants could be considered microphthalmic at this stage of development. At 3 dpf in the wild-type eye, the RPE had grown thicker and melanin synthesis and accumulation had increased, such that the RPE was dark black in appearance (Fig. 4H). Retinal lamination was largely complete, with only small non-laminated regions remaining at the CMZ. Photoreceptor mor-

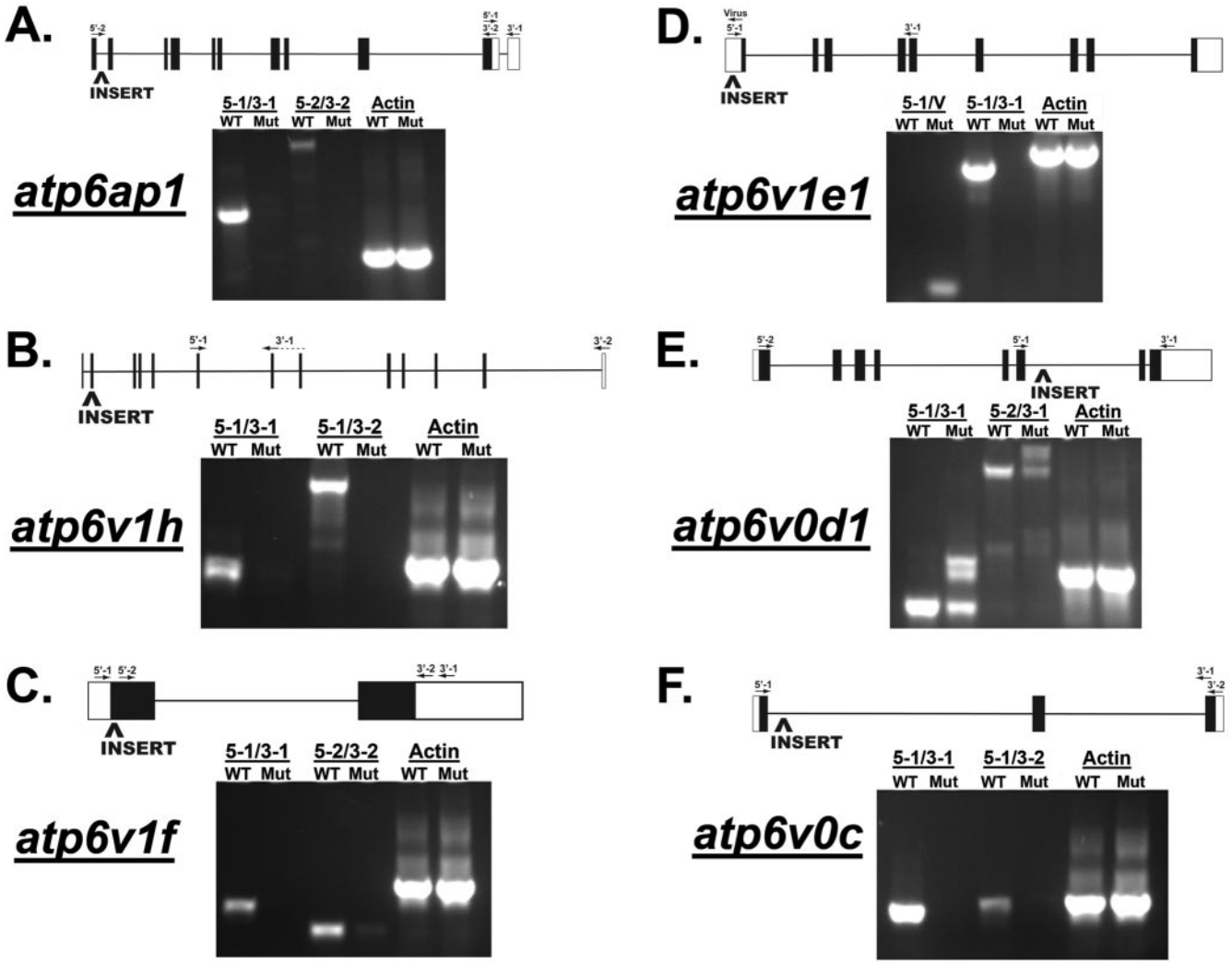

FIGURE 3. v-ATPase loci and gene expression in mutant embryos. Schematic representation of each v-ATPase locus (www.ensembl.org/Danio_rerio/[38]) with the approximate locations of the viral insertion and PCR primers used for assaying transcript levels. (**A**) The *atp6ap1* mutants contained a viral insertion in the first intron and had substantially less *atp6ap1* mRNA than did the wild-type embryos. (**B**) The *atp6v1h* mutants contained a viral insertion in the first intron and had no detectable *atp6v1h* mRNA. (**C**) The *atp6v1f* mutants contained a viral insertion in the first exon, 62 bp from the start codon, and possessed substantially less *atp6v1f* mRNA than wild-type embryos. (**D**) The *atp6v1e1* mutants had a viral insertion in the 5′ UTR, which was included in the *atp6v1e1* transcript. This resulted in truncation and possibly degradation of the transcripts in mutants. (**E**) The *atp6v0d1* mutants had a viral insertion in the sixth intron, which leads to aberrant mRNA splicing and the inclusion of the proviral insert in a portion of the transcripts. As a result, a translational frameshift occurred and the last 53 amino acids of the atp6v0d1 protein, encoded by exons 7 and 8, were replaced by the translated viral sequence. (**F**) *atp6v0c* mutants have a viral insertion in the first intron and have no detectable *atp6v0c* mRNA.

phogenesis was also well under way in the outer nuclear layer (ONL) with photoreceptor outer segments elongating and beginning to interdigitate with the RPE. In contrast, the v-ATPase mutant RPE remained hypopigmented relative to the wild-type RPE (Figs. 4I–N), and moreover, patches of nonpigmented RPE were observed in some mutants (Fig. 4I), whereas in others, large clumps of pigmented RPE were displaced into the ONL or the subretinal space (Fig. 4M). Mutant eyes remained microphthalmic and regions of pyknotic nuclei and acellular holes were observed within the retina (Fig. 4K) and near the CMZ (Fig. 4N) of some mutants, suggestive of increased levels of apoptosis.

At 5 dpf the wild-type eye had grown considerably and possessed all differentiated cell types (Fig. 4O). The RPE lined the posterior of the eye and microvilli interdigitated around the photoreceptor outer segments, to provide structural support. In v-ATPase mutants the RPE remained hypopigmented (Figs. 4P–U), except in *atp6v1e1* mutants, which had near-normal levels of pigmentation (Fig. 4S). In most mutants, RPE morphology was highly abnormal. In some eyes, patches of nonpigmented RPE were evident (Figs. 4P, 4T) and regions of clumped pigmented cells had invaded the retina (Fig. 4T). Retinal lamination appeared unaffected in all mutants except for *atp6v0c* (Fig. 4U); however, photoreceptor morphology was abnormal. In some mutants, photoreceptor outer segments were longer and/or disorganized (Figs. 4P′, 4Q′), whereas in others, outer segments were nearly absent (Figs. 4S′, 4U′). Mutant eyes remain microphthalmic, and regions of pyknotic nuclei continued to be observed near the CMZ in all mutants (Figs. 4P, 4Q, 4U) and throughout the *atp6v1f* retina (Fig. 4R).

Identification and Cloning of an ENU-Induced Allele of *atp6ap1*

a82 is a recessive mutation that was identified in an ENU-based forward genetic screen due to its severely hypopigmented body and RPE (Fig. 5A; Darland T, unpublished observations,

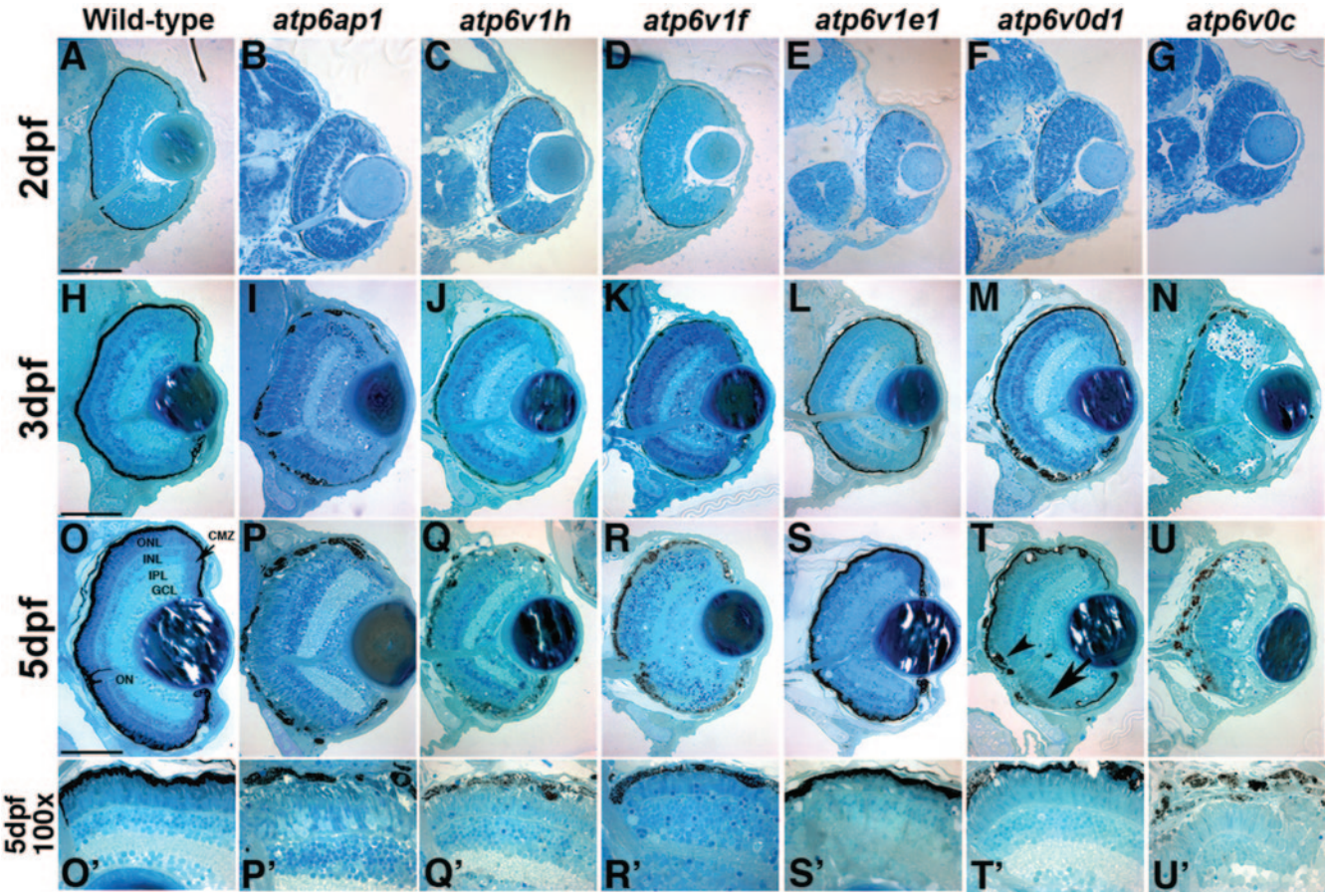

Figure 4. Histology of v-ATPase mutant eyes. v-ATPase mutants showed RPE and retinal defects. (**A**) Wild-type embryos possessed a mildly pigmented RPE at 2 dpf that became increasingly pigmented at 3 (**H**) and 5 (**O**) dpf as melanin levels rose. In wild-type embryos, the RPE was continuous, forming an epithelial layer encompassing the retina out to the retinal periphery. v-ATPase mutants showed very little RPE pigmentation at 2 dpf (**B–G**). Although pigment levels increased at 3 (**I–N**) and 5 (**P–U**) dpf in the mutants, they failed to reach wild-type levels in all but the *atp6v1e1* mutants (**L**, **S**). RPE morphology was significantly affected in the mutants in which large patches of RPE lacking pigmentation were apparent (**T**, *arrow*), and thickened clumps of RPE invaded the retina (**T**, *arrowhead*). Retinal patterning was also disrupted. Photoreceptor morphology was abnormal where photoreceptor outer segments were dramatically elongated in some mutants (**P′**, **T′**) and appeared underdeveloped or absent in others (**S′**, **U′**). Pyknotic nuclei and acellular holes were observed at the ciliary marginal zone (e.g., **P**, **Q**, **U**) and in the retina (**R**). Transverse sections, dorsal is up in all images. ONL, outer nuclear layer; INL, inner nuclear layer; IPL, inner plexiform layer; GCL, ganglion cell layer; CMZ, ciliary marginal zone; ON, optic nerve. Scale bars, 100 μm.

2000). *a82* mutant histology showed obvious RPE and retinal defects similar to those observed in v-ATPase mutants (Figs. 5B–D). Given the similarities in phenotype between the v-ATPase mutants and *a82*, we tested whether *a82* was allelic to any of the insertional v-ATPase mutations. Complementation crosses identified *atp6ap1* as a noncomplementing allele of *a82*, strongly suggesting that *a82* possesses a mutation in the *atp6ap1* gene. Cloning and sequencing of the *atp6ap1* locus in *a82* mutants revealed that *a82* mutants possessed a T→A nonsense mutation at position 317 of the *atp6ap1* coding sequence (Fig. 5E). This led to an L→X amino acid change and a premature stop codon at position 106 of the atp6ap1 protein, truncating it to 23% of the wild-type size. The *Drosophila*, bovine, mouse, zebrafish, and human atp6ap1 proteins all contain putative transmembrane domains at the C termini[40]; and this domain was eliminated in the *a82* mutants (Fig. 5E). We now refer to *a82* as *atp6ap1*^{a82}, in accordance with zebrafish nomenclature guidelines. We predict that the *atp6ap1*^{a82}-encoded fragment is nonfunctional and thus that *atp6ap1*^{a82} is a null allele.

For all subsequent experiments, data are presented from experiments performed on two of the v-ATPase mutants: *atp6ap1*and *atp6v0d1*. In all experiments on *atp6ap1*, the *atp6ap1*^{bi112} allele was used. Similar results were obtained in all assays from each of the other v-ATPase mutants, except where noted.

v-ATPase Expression

To begin to analyze the phenotypes present in v-ATPase mutant embryos and their underlying causes, we first sought to determine the relevant domains of v-ATPase expression in the developing embryo. RT-PCR on total RNA samples isolated from two-cell-stage embryos indicated that all the subunits are maternally provided (data not shown). In situ hybridization revealed overlapping regions of expression for each transcript at 24 hpf (Fig. 6 and data not shown). v-ATPase expression was observed in the RPE (Figs. 6A, 6C, 6E, 6F) and along the dorsal surface of the embryo, probably in neural crest–derived pigment cells (Figs. 6B, 6E). In addition, spots of expression were observed over the yolk, most likely the mucous cells that cover the surface of the embryo, and expression was also observed in the brain. Similar expression of these and additional v-ATPase subunit transcripts has also been reported in zebrafish.[30] No staining was observed in sense controls (data not shown).

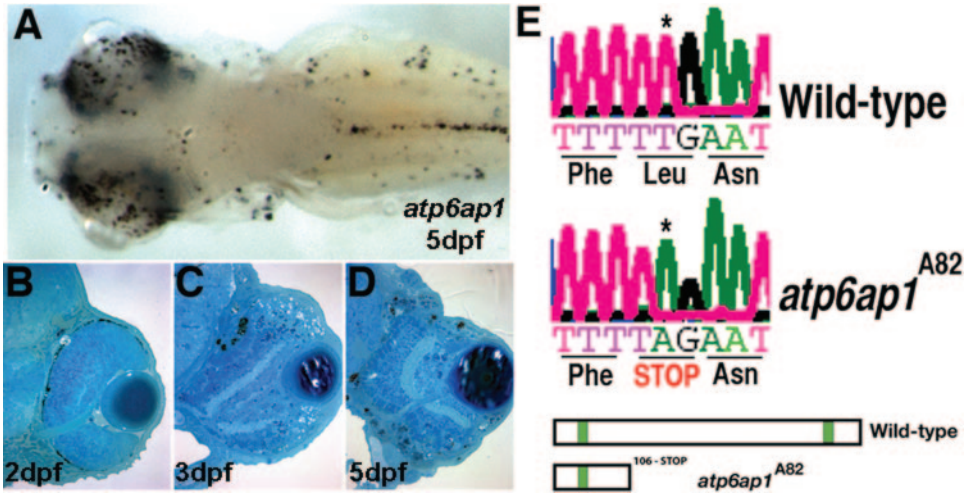

FIGURE 5. The *a82* mutant is an *atp6ap1* allele. (**A**) Recessive *a82* mutants are oculocutaneous albinos and microphthalmic. Shown is a dorsal view of an *a82* mutant at 5 dpf. (**B–D**) Transverse section histology of *a82* at 2 (**B**), 3 (**C**), and 5 (**D**) dpf revealed obvious retinal and RPE defects similar to those present in v-ATPase mutants. (**E**) *a82* mutants possessed a nonsense mutation (TTG → TAG) at bp317 of the *atp6ap1* coding sequence (**E**, *asterisk*). This led to a premature stop codon and truncation of the atp6ap1 protein at amino acid position 106 (L106X). (**B–D**) Dorsal is up.

Retinoblast Proliferation and Neuronal Apoptosis in v-ATPase Mutants

We next wanted to determine how loss of v-ATPase activity leads to microphthalmia. Three hypotheses that could account for the reduction in eye size are: reduced overall proliferation of cells within the optic cup and/or the CMZ, deficiencies in the timing of cell cycle exit, and/or increased cell death.

To test the first two of these hypotheses and assay retinoblast proliferation, we used BrdU incorporation to identify CMZ cells in the S-phase over the duration of BrdU exposure. The embryos were exposed to BrdU from 36 to 48, 48 to 60, and 72 to 96 hpf and were either fixed immediately (Figs. 7A–C, 7E–G, 7I–K) or washed clear of BrdU, allowed to grow for an additional 24 hours, and then fixed (Figs. 7D, 7H, 7L). This exposure and fixation regimen enabled identification of the total number of proliferative cells at 48 hpf, the earliest time at which the mutants can be phenotypically identified, and at 60 and 96 hpf, as well as an assessment of the subsequent number of divisions and survival of these cells between 96 and 120 dpf.

From 36 to 48 hpf, wild-type embryos possessed 172 ± 6 $BrdU^+$ cells (Fig. 7M), and most of these were distributed to the peripheral retina and the outer retinal regions (perspective INL/ONL; Fig. 7A). By comparison, the *atp6ap1* mutants possessed 198 ± 12 $BrdU^+$ cells and the *atp6v0d1* mutants possessed only 217 ± 16 (Fig. 7M), and these cells were localized throughout the entire retina (Figs. 7E, 7I). From 48 to 60 hpf, wild-type embryos possessed 143 ± 12 $BrdU^+$ cells (Fig. 7M), nearly all of which were located at the retinal periphery or in recently born photoreceptors (Fig. 7B). Over this period, *atp6ap1* mutants possessed 150 ± 15 $BrdU^+$ cells, while *atp6v0d1* mutants possessed 211 ± 13 (Fig. 7M). In the mutants, $BrdU^+$ cells were at their highest density at the retinal periphery; however, they also extended throughout the entire ONL as well as scattered throughout the INL (Figs. 7F, 7J). BrdU exposures from 72 to 96 hpf indicated that over this period, wild-type embryos possessed 58 ± 6 $BrdU^+$ cells (Fig. 7M), all located within the CMZ (Fig. 7C), while *atp6ap1* mutants possessed 38 ± 7 and *atp6v0d1* only 25 ± 5 $BrdU^+$ cells (Fig. 7M). All $BrdU^+$ cells were properly localized to the CMZ in the mutants at 96 hpf (Figs. 7G, 7K). By 5 dpf, differences between the mutants and wild-type siblings became more dramatic, and wild-type embryos possessed on average of 70 ± 6 $BrdU^+$ cells (Fig. 7M). During retinal growth, as CMZ cells exit the cell cycle and begin to differentiate they are coordinately displaced into the retina to eventually take their proper laminar position.[41] Thus, as expected, most of the $BrdU^+$ cells in wild-type embryos had begun to integrate centrally into the retina, concomitant with their differentiation as retinal neuron subtypes (Fig. 7D). In contrast to this, *atp6ap1* mutants possessed only 28 ± 9 $BrdU^+$ cells, and *atp6v0d1* mutants possessed only 23 ± 4 $BrdU^+$ cells (Fig. 7M). In addition, all the $BrdU^+$ cells in both mutants remained at the CMZ, none were localized within the retina (Figs. 7H, 7L).

Histologic examinations show an increase in pyknotic nuclei internal to the proliferative zone of the CMZ in v-ATPase mutants beginning at 3 dpf (Fig. 4); the location of these apoptotic foci internal to the highly proliferative zone of the CMZ suggests that they are CMZ-derived and that they are undergoing apoptosis during or just after their exit from the

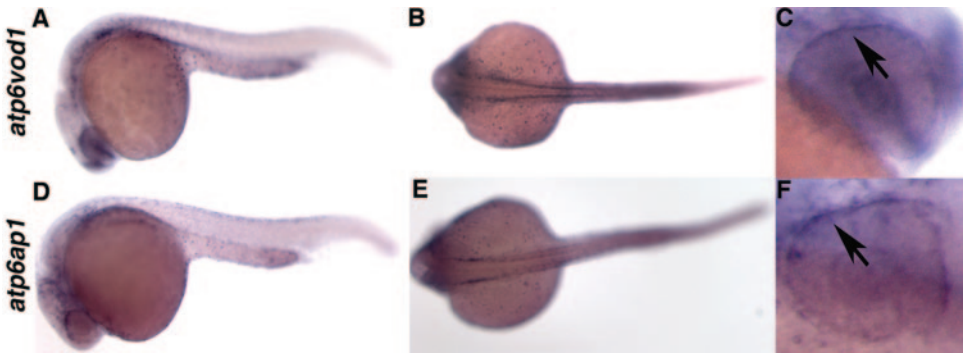

FIGURE 6. *atp6v0d1* (**A–C**) and *atp6ap1* (**D–F**) expression at 24 hpf was observed in the RPE and along the dorsal surface of the embryo, likely pigment cells. Expression was observed over the yolk, likely in the mucous cells that cover the surface of the embryo, and in the brain. (**C**, **F**) High magnification view indicating RPE expression (*arrows*).

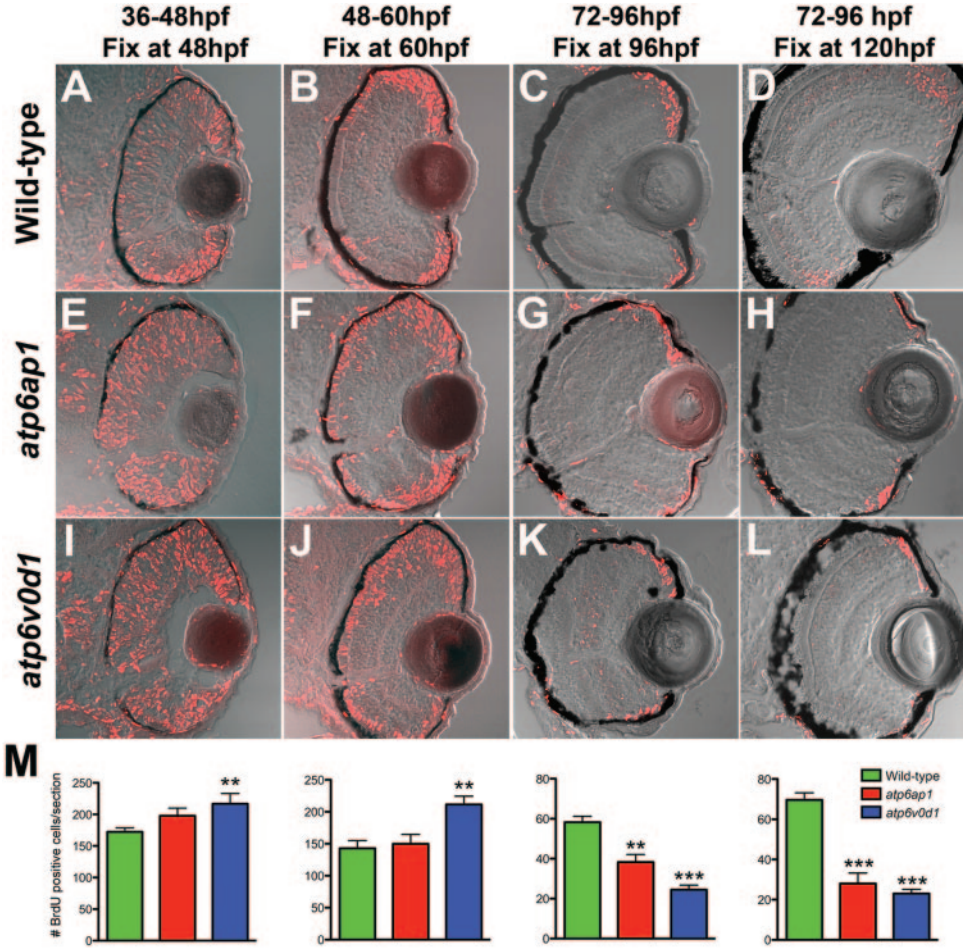

FIGURE 7. v-ATPase mutants exhibited defects in retinoblast proliferation. Wild-type (**A–D**), *atp6ap1* (**E–H**), and *atp6v0d1* (**I–L**) embryos were exposed to BrdU from 36 to 48 hpf (**A**, **E**, **I**), 48 to 60 hpf (**B**, **F**, **J**), 72 to 96 hpf, and either fixed at 96 hpf (**C**, **G**, **K**) or washed and fixed at 120 hpf (**D**, **H**, **L**). In wild-type embryos, at 48 hpf large regions of BrdU+ cells were found at the retinal periphery (**A**), and these regions refined down to the extreme retinal periphery over the next 48 hours (**B**, **C**) to comprise solely the dorsal and ventral CMZs. After a 24-hour "chase," $BrdU^+$ cells incorporated into the retina as they differentiated into neuronal subtypes (**D**). In contrast, in the v-ATPase mutant retina at 48 hpf, $BrdU^+$ cells were not limited to the retinal periphery (**E**, **I**), and in *atp6v0d1* mutants, they were observed in increased numbers when compared to wild-type (**M**; $P < 0.05$). Over the next 24 hours, some refinement occurred in the CMZ; however ectopic $BrdU^+$ cells were observed in the central retina at 60 hpf (**F**, **J**). The number of $BrdU^+$ cells also increased in the *atp6v0d1* mutant (**M**; $P < 0.05$). At 72 hpf, $BrdU^+$ cells were located at the CMZ (**G**, **K**) but their numbers are significantly lower in mutant eyes (**M**). (**D**) After a 24-hour chase (120 hpf), v-ATPase mutants still possessed $BrdU^+$ cells, but these were even further reduced in number (**M**) and most remained at the CMZ (**H**, **L**). (**M**) Quantification of the average number of BrdU+ cells per transverse section at each time point. Dorsal is up in all images.

cell cycle. To test the latter hypothesis for microphthalmia in the v-ATPase mutants, TUNEL staining was performed on wild-type and v-ATPase mutant retinas at 2, 3, and 5 dpf. Indeed, substantially higher levels of apoptosis were observed in the v-ATPase mutant retina (Fig. 8). No apoptotic nuclei were observed in wild-type or *atp6v0d1* mutant embryos at 2 dpf (Figs. 8A, 8I), and few were observed in *atp6ap1* mutants (Fig. 8E; 2.66 ± 3.09). At 3 dpf the levels of apoptosis rose dramatically in v-ATPase mutants relative to wild-type siblings with *atp6v0d1* mutants possessing, on average, 47 ± 13.9 $TUNEL^+$ cells and *atp6ap1* mutants possessing 46 ± 5.7 (Figs. 8B, 8F, 8J). $TUNEL^+$ cells were observed throughout the v-ATPase mutant retina and were concentrated in distinct foci internal from the proliferative zone of the CMZ at both the dorsal and ventral retinal margins (Figs. 8F, 8J). High levels of apoptosis at the CMZ continued in the mutant eye through 5 dpf with *atp6v0d1* mutants possessing, on average, 31.3 ± 9.4 $TUNEL^+$ cells, and *atp6ap1* mutants possessing 16.3 ± 7.6 (Figs. 8C, 8G, 8K). Elevated numbers of apoptotic cells were also observed throughout the *atp6v1f* retina at 5 dpf (data not shown).

Morpholino knockdown of the *atp6v0a1* subunit in zebrafish leads to deficiencies in microglial-mediated mediated neuronal degradation and clearance of apoptotic neurons within the zebrafish brain.[24] Loss of atp6v0a1 function was not reported to lead to increased levels of apoptosis in the brain, however. In each of the v-ATPase mutants described, when compared to wild-type siblings, substantial increases in $TUNEL^+$ cells were observed scattered throughout the brain (Figs. 8D, 8H, 8L), as well as in distinct foci adjacent to the ventricular zone (Fig. 8H). In addition, apoptotic cells were often observed in clusters where six to seven $TUNEL^+$ cells were located in close proximity to one another (Figs. 8H, 8L).

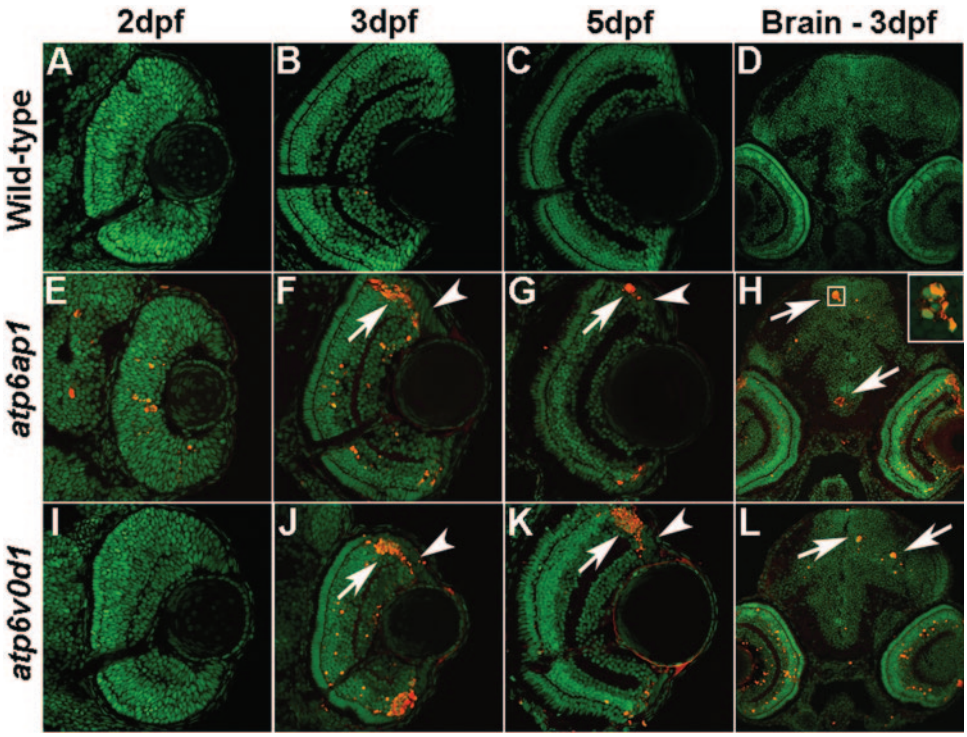

FIGURE 8. v-ATPase mutants exhibited increased levels of apoptosis in the CMZ and brain. Wild-type embryos exhibited few TUNEL$^+$ cells in their eye at 2 (**A**), 3 (**B**), or 5 (**C**) dpf. Conversely, v-ATPase mutants showed increased levels of apoptosis. Several TUNEL$^+$ cells were observed in the *atp6ap1* mutants as early as 2 dpf (**E**), whereas few were found in the *atp6v0d1* mutants (**I**). Apoptosis rose dramatically in both mutants at 3 dpf (**F**, **J**) with scattered cells observed throughout the retina and concentrated apoptotic regions (**F**, **J**, *arrows*) localized internal to the ciliary marginal zones (**F**, **J**, *arrowheads*). (**G**, **K**) Apoptotic cells (*arrows*) continued to be observed internal to the ciliary margin (*arrowheads*) through 5 dpf. An increased numbers of apoptotic cells are also frequently observed in the v-ATPase mutant brain (*arrows* in **H**, **L**) in comparison to the wild-type brain (**D**) at 3 dpf. Apoptotic cells are often found in clusters (*inset*: high-magnification view of boxed region in **H**). Transverse sections; dorsal is up in all images.

Disorganization of the ONL in v-ATPase Mutants

We next wanted to further examine retinal patterning in v-ATPase mutants using immunohistochemical markers for retinal neuron subtypes (Fig. 9). All retinal cell types were present in the v-ATPase mutant retina and lamination was normal (Figs. 9A–C and data not shown). However, as suggested from histology, ONL morphology was disrupted (Figs. 9D–L). Staining for both 1d1, a marker of rods (Figs. 9D–F), and zpr-1, a marker of red-green double cones[42] demonstrated the presence of numerous folds or rosettes of photoreceptors in the mutant retina. Photoreceptors within these regions formed outer segments, but they were disheveled in appearance when compared with control outer segment morphology (Figs. 9D–I), and they were not oriented perpendicularly to the RPE (Fig. 9I). Superimposing zpr-1 and DIC images revealed that the photoreceptors in these disrupted regions were no longer apposed to the RPE but rather they were localized more internally within the retina, adjacent to what appeared to be either

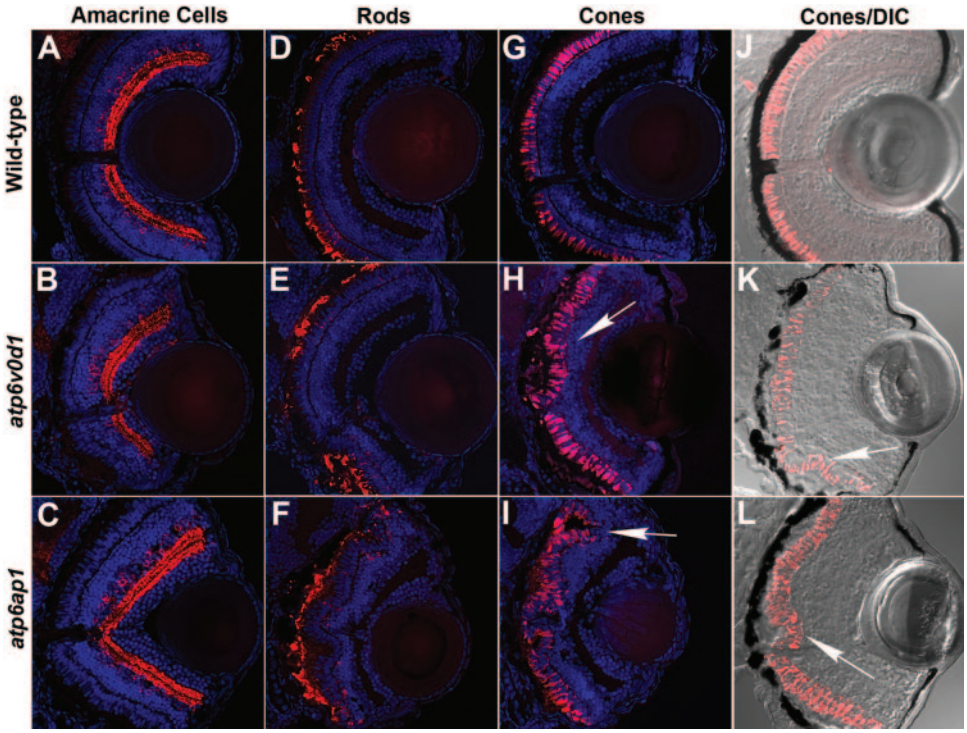

FIGURE 9. v-ATPase mutants exhibited disorganization of the ONL. (**A–C**) 5e11 staining of amacrine cells indicated that these cells were present and patterned normally in the v-ATPase retina. Similar results were obtained for retinal ganglion cells and bipolar cells (data not shown). Rod staining with 1d1 (**D–F**) and red–green double cone staining with zpr-1 (**G–I**) indicated that although the rods and cones were present, ONL morphology was disrupted. Rosette-like structures of photoreceptors were observed in the mutant ONL (**H**, **I**, *arrows*). Overlaying zpr-1 staining with DIC images indicates that the most disrupted ONL regions correlate with regions of abnormal RPE morphology (*arrows* in **K**, **L**). *Red*: antibody staining; *blue*: nuclei. Transverse sections; dorsal is up in all images.

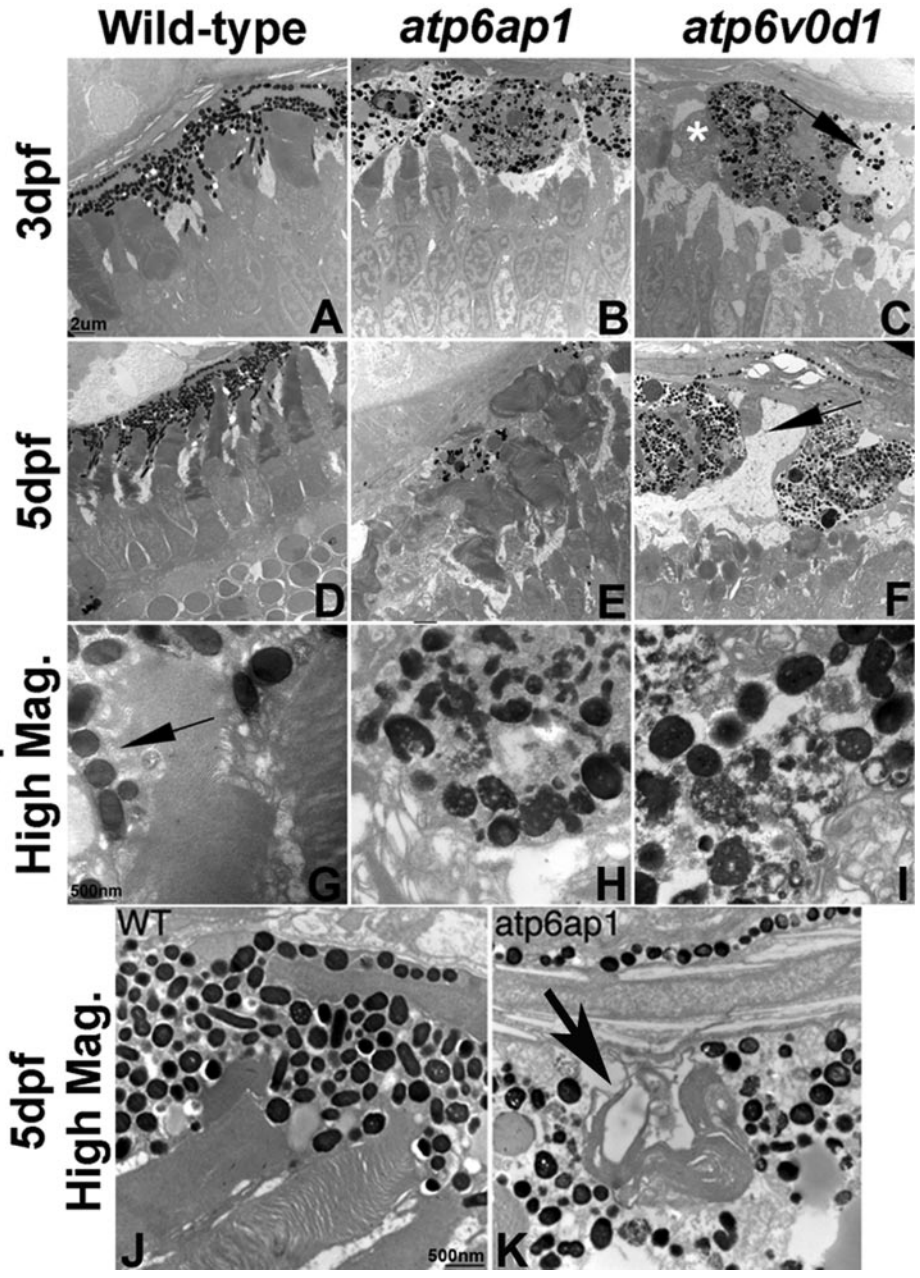

FIGURE 10. Ultrastructural analysis of the v-ATPase mutant retina and RPE. TEM of transverse sections from wild-type (**A**, **D**, **G**, **J**), *atp6ap1* (**B**, **E**, **H**, **K**), and *atp6v0d1* (**C**, **F**, **I**) mutant embryos. (**A**) At 3 dpf, the wild-type RPE was a compact epithelial layer filled with melanosomes. (**B**, **C**) The RPE in the v-ATPAse mutants was much wider and appeared malformed. Melanosome formation and/or survival was abnormal, with the melanosomes much smaller in size and appearing to have ruptured. Undigested photoreceptor outer segments were evident in the mutant RPE (**C**, *asterisk*) and large vacuolated regions are present in the mutant RPE (**C**, *arrow*). Cone outer segments have formed, but they were not tightly apposed to the RPE as they were in the wild-type. (**D**, **G**, **J**) At 5 dpf, the wild-type RPE had attained a mature morphology where microvilli extended and interdigitated between photoreceptor outer segments (**G**, *arrow*). (**E**, **F**, **H**, **I**, **K**) In mutants, the RPE was substantially thicker than that in the wild-type, with large vacuolated regions evident (**F**, *arrow*). No RPE microvilli were observed. Photoreceptor outer segments were malformed and disheveled in appearance, and shed discs were observed in membrane-bound vacuoles throughout the RPE (**K**, *arrow*). (**H**, **I**) Melanosomes were abnormal in shape and appeared underdeveloped or to have ruptured.

gaps between the retina and RPE, and/or regions of morphologically abnormal RPE (Figs. 9J–L). In addition, as suggested from histology (Figs. 4S, S′), many photoreceptors in *atp6v1e1* mutants lacked 1d1 and zpr-1 stained outer segments (data not shown).

To gain a high-resolution view of the photoreceptor and RPE defects, we next performed transmission electron microscopy (TEM) on ultrathin sections cut from wild-type and *atp6ap1* and *atp6v0d1* mutants (Fig. 10). At 3 dpf, wild-type photoreceptor outer segments were positioned adjacent to the RPE, and they grew toward it perpendicularly (Fig. 10A). By 5 dpf, wild-type outer segments had grown considerably and had interdigitated into the RPE where pigmented microvilli extended from the RPE to surround individual outer segments (Figs. 10D, 10G). By comparison, at 3 dpf, v-ATPase mutant photoreceptors were rarely observed adjacent to RPE cells; rather, they projected around regions of bloated RPE and were separated from the RPE by gaps of one to several hundred nanometers (Figs. 10B, 10C). By 5 dpf, photoreceptor morphologies were highly abnormal; the outer segments were disorganized and disheveled in appearance (Figs. 10E, 10F). Mutant RPE was disrupted, in comparison to the RPE of wild-type embryos, which is a continuous epithelium ~ 2.5 μm wide and filled with thousands of smooth-edged melanosomes (Figs. 10A, 10D). The mutant RPE, when present, was much thicker (~10 μm on average) and its morphology was highly abnormal (Figs. 10E, 10F, 10H, 10I). Mutant RPE cells also often contained large intracellular membrane-bound vacuoles (Figs. 10C, 10F), possibly lysosomal in origin, that contained fragments of undigested outer segment material (Fig. 10K). Melanosome formation was compromised in v-ATPase mutants where their morphology was highly abnormal, and they appeared either to have failed to properly mature into smooth-edged melanosomes or to have ruptured at some point during their morphogenesis (Figs. 10H, 10I).

Discussion

In this study, we characterized the ocular defects in seven recessive zebrafish v-ATPase mutants that disrupt five different core subunits of the v-ATPase complex, and a v-ATPase associated protein. In addition, morpholino-induced phenotypes for *atp6v0b* and *atp6v0c* have also been reported, and these closely resemble the mutant phenotypes described herein.[36,43] Zebrafish v-ATPase mutants are oculocutaneous albinos and, in the RPE, this is likely to result from combined defects in melanosome formation, localization, and survival. The RPE is severely disrupted in v-ATPase mutants with some regions of the eye lacking visible RPE altogether, leading to an overall patchiness in eye pigmentation in the mutants. In addition, where present, the RPE is bloated and appears to be malformed. Melanosomes are present in these RPE regions; however, they are hypopigmented and many appear also to be malformed, or to have ruptured.

The v-ATPase complex plays key roles in the acidification of lysosomes and endosomes.[21] Melanosomes are lysosome-related organelles and several reports have detailed the similarities in biogenesis and cellular functions between these organelles.[44–46] Like lysosomes, melanosomes are acidic organelles with intracellular pH values as low as 4.0.[47] Several studies have suggested that melanogenesis is dependent on a low intracellular pH, as experimental disruption of the pH gradient across melanosomes results in defects in melanin levels and in overall melanosome morphology.[48–50] Other studies have suggested instead that melanogenesis occurs at a neutral pH and that decreases in melanosomal pH actually inhibit the enzymes required for melanin synthesis.[51–54] We do not yet know the pH of melanosomes in the v-ATPase mutant RPE, and attempts at measuring this in vivo with pH-sensitive dyes have been thus far unsuccessful (data not shown). Given the role of the v-ATPase complex in numerous acidification events in other biological contexts, however, our results seem to support the former of these hypotheses. Additional studies are needed to determine how the regulation of melanosomal pH influences vertebrate melanogenesis and melanosome biogenesis and to determine whether mutations in v-ATPase subunits underlie any ocular or oculocutaneous albinism disorders in humans.

The v-ATPase mutants appeared microphthalmic and from the combined results of BrdU and TUNEL assays, our data suggest that the microphthalmia results from several distinct, but probably related, defects in the mutant eye. First, increased numbers and ectopically located proliferative retinoblasts were observed in mutants at 48 and 60 hpf (Fig. 7). v-ATPase mutants may simply be developmentally delayed, and because of this, the retinoblast cell cycle exit is slower than that in wild-type siblings. Conversely, v-ATPase complex function may be required for the exit of retinoblasts from the cell cycle for them to differentiate at the appropriate time. Indeed, from histologic examination, retinal lamination was slightly delayed at 2 dpf in the mutant eye, suggesting that neuronal differentiation is impaired in the mutants. At later time points, however, a decreased number of proliferating cells was observed in the CMZ, and these are concomitant with increased levels of apoptosis in the retina (Figs. 7, 8). Apoptotic cells were located internally in the retina, relative to the CMZ, suggesting that it is newly born retinal neurons undergoing apoptosis, not the proliferative cells of the CMZ. Collectively, these observations suggest two distinct roles for the v-ATPase complex in regulating later phase, CMZ-dependent retinal growth: v-ATPase function may be required for the maintained proliferation within the CMZ, and v-ATPase function may also be required for the survival of newly generated CMZ-derived retinal neurons. An alternative hypothesis that cannot as yet be ruled out is that the mutant CMZ continues to generate new cells, but at a slower rate, proportional to the decreased eye size that results solely from the increased levels of apoptosis in the mutants. That said, while scattered apoptotic cells were observed throughout the retinas of some of the mutants, surprisingly their numbers were few in most, and it is doubtful that this alone could explain the microphthalmia.

While additional experiments are necessary to fully determine the role of the v-ATPase complex during eye development, two testable models can be provided that could explain how the v-ATPase complex may mediate these proliferative and survival functions during eye formation, and these models are not mutually exclusive. (1) v-ATPase complex activity could be *directly* necessary within retinoblasts, to regulate their on-time cell cycle exit, and at later time points at the CMZ for maintained proliferation and survival of newly generated neurons. (2) v-ATPase complex activity could be essential for the normal development and function of the RPE, and ocular defects observed in the mutants could thereby stem *indirectly* from malformation, or hypopigmentation, of the RPE. Because v-ATPase transcripts were enriched in cells of the RPE (Fig. 6[30]) and the RPE is known to play many important roles in regulating development of the retina, we favor the latter of these hypotheses. Indeed, in support of this notion, several other zebrafish mutations that affect the RPE display defects similar to those described herein for the v-ATPase mutants (e.g., Refs. 55, 56).

Several growth factors and neurotransmitters are secreted by the RPE that could influence retinoblast proliferation and survival,[1,57] and RPE pigmentation has been proposed to play a direct role in regulating the rate of cell division within the developing retina.[1,58–61] These studies suggest that hypopigmentation of the RPE lengthens the retinoblast cell cycle thereby decreasing the rate of proliferation within the retinal neuroepithelium and resulting in smaller overall eye size. The molecular mechanisms underlying this effect are not known; however, one possibility is that ATP released from the RPE can regulate the rate of cell division in the adjacent retina.[58] If ATP levels were compromised in the v-ATPase mutant RPE due to hypopigmentation and/or RPE malformation, it could manifest during early eye formation as abnormal retinoblast proliferation. Similarly, the absence of RPE-derived growth factors could compromise the survival of newly generated neurons internal to the CMZ. Further experiments are necessary to determine whether the v-ATPase complex functions in regulating the proliferation and survival of retinal cells.

v-ATPase mutants possess obvious defects in photoreceptor morphogenesis where outer segments are malformed and photoreceptors are often observed to be associated in small groups, or rosettes, physically displaced from the abnormal RPE. Given the expression of v-ATPase subunits within the developing RPE, what is known about v-ATPase functions in other biological contexts, and, again, what is known with regard to RPE–retinal interactions, it is likely that the molecular mechanism underlying the photoreceptor defects in v-ATPase mutants stems indirectly from v-ATPase complex–dependent deficiencies within the RPE, rather than from direct roles for the complex within the photoreceptors. The RPE plays an integral role in photoreceptor maintenance, in part, by phagocytosing and degrading their continually growing outer segments in a circadian fashion.[10] In patients with age-related macular degeneration (ARMD), ingested photoreceptor outer segments are not readily degraded by the RPE, resulting in a buildup of lipofuscin and one of its principal components, A2E.[62–64] A2E accumulation in RPE lysosomes inhibits their ability to degrade outer segment debris and thus, this accumulation is thought to play a causative role in the progression of

ARMD.[65] The molecular mechanism of A2E-dependent RPE dysfunction is not currently known, but one hypothesis is that A2E inhibits the v-ATPase thereby preventing lysosomal acidification and protein/lipid degradation in RPE cells.[66] v-ATPase mutants display a buildup of undigested outer segment debris in enlarged vacuoles within their RPE, and the most parsimonious explanation is that these vacuoles are lysosomal in origin. Because of a deficiency in v-ATPase-dependent lysosomal acidification, lysosomal proteases remain inactive and ingested outer segments are not efficiently degraded, which leads to a poisoning of the RPE cell and, over time, an inability of these cells to continue to maintain the adjacent photoreceptors. Indeed, in vitro studies in cultured rat RPE cells support this hypothesis, and these studies have shown that that inhibition of the v-ATPase pump by bafilomycin A does not affect outer segment phagocytosis; rather, it leads to a buildup of ingested and undegraded outer segment debris.[67]

As discussed earlier, several other mutants have been identified in zebrafish that present with ocular phenotypes similar to those described for the v-ATPase mutants. These include *fading vision*, which disrupts the *silver* gene encoding a protein that is essential for intraluminal fibril formation in melanosomes[56]; *leberknodel*, which disrupts the *Vam6p/Vps39p* gene encoding a protein component of the HOPS complex, which is necessary for lysosomal tethering and fusion[55]; and *rep1*, encoding Rab-escort protein 1, which is essential for posttranslational modification of Rab proteins.[68,69] In addition there are several as-yet-uncloned mutations with ocular phenotypes resembling the v-ATPase mutations. These include *gantenbein*, *bleached*, *fade out*, *piegus*, *punktata*, and *mizierny*, which have yet to be positionally cloned.[55,70–73] Each of these mutations has in common with the v-ATPase mutants a severe RPE hypopigmentation associated with RPE malformations and degeneration and defects in photoreceptor morphogenesis and survival. Photoreceptor defects in two of these mutants, *fading vision* and *rep1*, have been shown to result from defects in the RPE,[56,69] and therefore it will be interesting to assay the autonomy of v-ATPase complex function in the zebrafish eye, as it relates to photoreceptor morphogenesis, as well as retinoblast proliferation and survival in the CMZ, to determine whether v-ATPase complex function is indeed the mediator within RPE cells of these developmental events.

Acknowledgments

The authors thank Adam Amsterdam and Nancy Hopkins for providing the v-ATPase mutant fish and Will Coe for technical assistance.

References

1. Strauss O. The retinal pigment epithelium in visual function. *Physiol Rev.* 2005;85:845–881.
2. Raymond SM, Jackson IJ. The retinal pigmented epithelium is required for development and maintenance of the mouse neural retina. *Curr Biol.* 1995;5:1286–1295.
3. Jensen AM, Walker C, Westerfield M. mosaic eyes: a zebrafish gene required in pigmented epithelium for apical localization of retinal cell division and lamination. *Development.* 2001;128:95–105.
4. Jensen AM, Westerfield M. Zebrafish mosaic eyes is a novel FERM protein required for retinal lamination and retinal pigmented epithelial tight junction formation. *Curr Biol.* 2004;14:711–717.
5. Gu SM, Thompson DA, Srikumari CR, et al. Mutations in RPE65 cause autosomal recessive childhood-onset severe retinal dystrophy. *Nat Genet.* 1997;17:194–197.
6. Marlhens F, Bareil C, Griffoin JM, et al. Mutations in RPE65 cause Leber's congenital amaurosis. *Nat Genet.* 1997;17:139–141.
7. Petrukhin K, Koisti MJ, Bakall B, et al. Identification of the gene responsible for Best macular dystrophy. *Nat Genet.* 1998;19:241–247.
8. Zarbin MA. Current concepts in the pathogenesis of age-related macular degeneration. *Arch Ophthalmol.* 2004;122:598–614.
9. Marmorstein AD, Finnemann SC, Bonilha VL, Rodriguez-Boulan E. Morphogenesis of the retinal pigment epithelium: toward understanding retinal degenerative diseases. *Ann N Y Acad Sci.* 1998; 857:1–12.
10. Matsumoto B, Defoe DM, Besharse JC. Membrane turnover in rod photoreceptors: ensheathment and phagocytosis of outer segment distal tips by pseudopodia of the retinal pigment epithelium. *Proc R Soc Lond B Biol Sci.* 1987;230:339–354.
11. Schraermeyer U, Heimann K. Current understanding on the role of retinal pigment epithelium and its pigmentation. *Pigment Cell Res.* 1999;12:219–236.
12. Carden SM, Boissy RE, Schoettker PJ, Good WV. Albinism: modern molecular diagnosis. *Br J Ophthalmol.* 1998;82:189–195.
13. Lyle WM, Sangster JO, Williams TD. Albinism: an update and review of the literature. *J Am Optom Assoc.* 1997;68:623–645.
14. Oetting WS, Brilliant MH, King RA. The clinical spectrum of albinism in humans. *Mol Med Today.* 1996;2:330–335.
15. Oetting WS, King RA. Molecular basis of albinism: mutations and polymorphisms of pigmentation genes associated with albinism. *Hum Mutat.* 1999;13:99–115.
16. Oetting WS, Summers CG, King RA. Albinism and the associated ocular defects. *Metab Pediatr Syst Ophthalmol.* 1994;17:5–9.
17. Kinnear PE, Jay B, Witkop CJ Jr. Albinism. *Surv Ophthalmol.* 1985;30:75–101.
18. Kriss A, Russell-Eggitt I, Harris CM, Lloyd IC, Taylor D. Aspects of albinism. *Ophthalmic Paediatr Genet.* 1992;13:89–100.
19. Amsterdam A, Nissen RM, Sun Z, Swindell EC, Farrington S, Hopkins N. Identification of 315 genes essential for early zebrafish development. *Proc Natl Acad Sci U S A.* 2004;101:12792–12797.
20. Gross JM, Perkins BD, Amsterdam A, et al. Identification of zebrafish insertional mutants with defects in visual system development and function. *Genetics.* 2005;170:245–261.
21. Nishi T, Forgac M. The vacuolar (H+)-ATPases–nature's most versatile proton pumps. *Nat Rev Mol Cell Biol.* 2002;3:94–103.
22. Nelson N, Harvey WR. Vacuolar and plasma membrane proton-adenosinetriphosphatases. *Physiol Rev.* 1999;79:361–385.
23. Adams DS, Robinson KR, Fukumoto T, et al. Early, H+-V-ATPase-dependent proton flux is necessary for consistent left-right patterning of non-mammalian vertebrates. *Development.* 2006;133: 1657–1671.
24. Peri F, Nusslein-Volhard C. Live imaging of neuronal degradation by microglia reveals a role for v0-ATPase a1 in phagosomal fusion in vivo. *Cell.* 2008;133:916–927.
25. Hiesinger PR, Fayyazuddin A, Mehta SQ, et al. The v-ATPase V0 subunit a1 is required for a late step in synaptic vesicle exocytosis in Drosophila. *Cell.* 2005;121:607–620.
26. Liegeois S, Benedetto A, Garnier JM, Schwab Y, Labouesse M. The V0-ATPase mediates apical secretion of exosomes containing Hedgehog-related proteins in Caenorhabditis elegans. *J Cell Biol.* 2006;173:949–961.
27. Alper SL. Genetic diseases of acid-base transporters. *Annu Rev Physiol.* 2002;64:899–923.
28. Basrur V, Yang F, Kushimoto T, et al. Proteomic analysis of early melanosomes: identification of novel melanosomal proteins. *J Proteome Res.* 2003;2:69–79.
29. Tabata H, Kawamura N, Sun-Wada GH, Wada Y. Vacuolar-type H(+)-ATPase with the a3 isoform is the proton pump on premature melanosomes. *Cell Tissue Res.* 2008;332:447–460.
30. Thisse B, Thisse C. Fast Release Clones: a high throughput expression analysis. Direct data submission. *ZFIN.* 2004, available at http://www.zfin.org. Accessed November 1, 2006.
31. Schredelseker J, Pelster B. Isoforms vatB1 and vatB2 of the vacuolar type ATPase subunit B are differentially expressed in embryos of the zebrafish (Danio rerio). *Dev Dyn.* 2004;230:569–575.
32. Kimmel CB, Ballard WW, Kimmel SR, Ullmann B, Schilling TF. Stages of embryonic development of the zebrafish. *Dev Dyn.* 1995;203:253–310.
33. Nuckels RJ, Gross JM. Histological preparation of embryonic and adult zebrafish eyes. *CSH Protocols.* 2007;doi:10.1101/pdb.prot4846.

34. Jowett T, Lettice L. Whole-mount in situ hybridizations on zebrafish embryos using a mixture of digoxigenin- and fluorescein-labelled probes. *Trends Genet.* 1994;10:73–74.
35. Uribe RA, Gross JM. Immunohistochemistry on cryosections from embryonic and adult zebrafish eyes. *CSH Protocols.* 2007;doi: 10.1101/pdb.prot4779.
36. Lee J, Willer JR, Willer GB, Smith K, Gregg RG, Gross JM. Zebrafish blowout provides genetic evidence for Patched1-mediated negative regulation of Hedgehog signaling within the proximal optic vesicle of the vertebrate eye. *Dev Biol.* 2008;319:10–22.
37. Golling G, Amsterdam A, Sun Z, et al. Insertional mutagenesis in zebrafish rapidly identifies genes essential for early vertebrate development. *Nat Genet.* 2002;31:135–140.
38. Hubbard T, Barker D, Birney E, et al. The Ensembl genome database project. *Nucleic Acids Res*. 2002;30:38–41
39. Kawasaki-Nishi S, Nishi T, Forgac M. Proton translocation driven by ATP hydrolysis in V-ATPases. *FEBS Lett.* 2003;545:76–85.
40. Supek F, Supekova L, Mandiyan S, Pan YC, Nelson H, Nelson N. A novel accessory subunit for vacuolar H(+)-ATPase from chromaffin granules. *J Biol Chem.* 1994;269:24102–24106.
41. Harris WA, Perron M. Molecular recapitulation: the growth of the vertebrate retina. *Int J Dev Biol.* 1998;42:299–304.
42. Larison KD, Bremiller R. Early onset of phenotype and cell patterning in the embryonic zebrafish retina. *Development.* 1990;109: 567–576.
43. Pickart MA, Sivasubbu S, Nielsen AL, Shriram S, King RA, Ekker SC. Functional genomics tools for the analysis of zebrafish pigment. *Pigment Cell Res.* 2004;17:461–470.
44. Dell'Angelica EC, Mullins C, Caplan S, Bonifacino JS. Lysosome-related organelles. *FASEB J.* 2000;14:1265–1278.
45. Marks MS, Seabra MC. The melanosome: membrane dynamics in black and white. *Nat Rev Mol Cell Biol.* 2001;2:738–748.
46. Seiji M, Fitzpatrick TB, Birbeck MS. The melanosome: a distinctive subcellular particle of mammalian melanocytes and the site of melanogenesis. *J Invest Dermatol.* 1961;36:243–252.
47. Puri N, Gardner JM, Brilliant MH. Aberrant pH of melanosomes in pink-eyed dilution (p) mutant melanocytes. *J Invest Dermatol.* 2000;115:607–613.
48. Ancans J, Tobin DJ, Hoogduijn MJ, Smit NP, Wakamatsu K, Thody AJ. Melanosomal pH controls rate of melanogenesis, eumelanin/phaeomelanin ratio and melanosome maturation in melanocytes and melanoma cells. *Exp Cell Res.* 2001;268:26–35.
49. Bhatnagar V, Anjaiah S, Puri N, Darshanam BN, Ramaiah A. pH of melanosomes of B 16 murine melanoma is acidic: its physiological importance in the regulation of melanin biosynthesis. *Arch Biochem Biophys.* 1993;307:183–192.
50. Tripathi RK, Chaya Devi C, Ramaiah A. pH-dependent interconversion of two forms of tyrosinase in human skin. *Biochem J.* 1988; 252:481–487.
51. Hearing VJ, Ekel TM. Mammalian tyrosinase: a comparison of tyrosine hydroxylation and melanin formation. *Biochem J.* 1976; 157:549–557.
52. Saeki H, Oikawa A. Stimulation by ionophores of tyrosinase activity of mouse melanoma cells in culture. *J Invest Dermatol.* 1985;85: 423–425.
53. Townsend D, Guillery P, King RA. Optimized assay for mammalian tyrosinase (polyhydroxyl phenyloxidase). *Anal Biochem.* 1984; 139:345–352.
54. Watabe H, Valencia JC, Yasumoto K, et al. Regulation of tyrosinase processing and trafficking by organellar pH and by proteasome activity. *J Biol Chem.* 2004;279:7971–7981.
55. Schonthaler HB, Fleisch VC, Biehlmaier O, et al. The zebrafish mutant lbk/vam6 resembles human multisystemic disorders caused by aberrant trafficking of endosomal vesicles. *Development.* 2008;135:387–399.
56. Schonthaler HB, Lampert JM, von Lintig J, Schwarz H, Geisler R, Neuhauss SC. A mutation in the silver gene leads to defects in melanosome biogenesis and alterations in the visual system in the zebrafish mutant fading vision. *Dev Biol.* 2005;284:421–436.
57. Martins RA, Pearson RA. Control of cell proliferation by neurotransmitters in the developing vertebrate retina. *Brain Res.* 2008; 1192:37–60.
58. Pearson RA, Dale N, Llaudet E, Mobbs P. ATP released via gap junction hemichannels from the pigment epithelium regulates neural retinal progenitor proliferation. *Neuron.* 2005;46:731–744.
59. Pearson R, Catsicas M, Becker D, Mobbs P. Purinergic and muscarinic modulation of the cell cycle and calcium signaling in the chick retinal ventricular zone. *J Neurosci.* 2002;22:7569–7579.
60. Ilia M, Jeffery G. Delayed neurogenesis in the albino retina: evidence of a role for melanin in regulating the pace of cell generation. *Brain Res Dev Brain Res.* 1996;95:176–183.
61. Rachel RA, Dolen G, Hayes NL, et al. Spatiotemporal features of early neuronogenesis differ in wild-type and albino mouse retina. *J Neurosci.* 2002;22:4249–4263.
62. Eldred GE, Lasky MR. Retinal age pigments generated by self-assembling lysosomotropic detergents. *Nature.* 1993;361:724–726.
63. Feeney-Burns L, Berman ER, Rothman H. Lipofuscin of human retinal pigment epithelium. *Am J Ophthalmol.* 1980;90:783–791.
64. Feeney-Burns L, Eldred GE. The fate of the phagosome: conversion to 'age pigment' and impact in human retinal pigment epithelium. *Trans Ophthalmol Soc U K.* 1983;103:416–421.
65. Finnemann SC, Leung LW, Rodriguez-Boulan E. The lipofuscin component A2E selectively inhibits phagolysosomal degradation of photoreceptor phospholipid by the retinal pigment epithelium. *Proc Natl Acad Sci U S A.* 2002;99:3842–3847.
66. Bergmann M, Schutt F, Holz FG, Kopitz J. Inhibition of the ATP-driven proton pump in RPE lysosomes by the major lipofuscin fluorophore A2-E may contribute to the pathogenesis of age-related macular degeneration. *FASEB J.* 2004;18:562–564.
67. Deguchi J, Yamamoto A, Yoshimori T, et al. Acidification of phagosomes and degradation of rod outer segments in rat retinal pigment epithelium. *Invest Ophthalmol Vis Sci.* 1994;35:568–579.
68. Starr CJ, Kappler JA, Chan DK, Kollmar R, Hudspeth AJ. Mutation of the zebrafish choroideremia gene encoding Rab escort protein 1 devastates hair cells. *Proc Natl Acad Sci U S A.* 2004;101:2572–2577.
69. Krock BL, Bilotta J, Perkins BD. Noncell-autonomous photoreceptor degeneration in a zebrafish model of choroideremia. *Proc Natl Acad Sci U S A.* 2007;104:4600–4605.
70. Biehlmaier O, Neuhauss SC, Kohler K. Double cone dystrophy and RPE degeneration in the retina of the zebrafish gnn mutant. *Invest Ophthalmol Vis Sci.* 2003;44:1287–1298.
71. Bahadori R, Rinner O, Schonthaler HB, et al. The Zebrafish fade out mutant: a novel genetic model for Hermansky-Pudlak syndrome. *Invest Ophthalmol Vis Sci.* 2006;47:4523–4531.
72. Neuhauss SC, Seeliger MW, Schepp CP, Biehlmaier O. Retinal defects in the zebrafish bleached mutant. *Doc Ophthalmol.* 2003; 107:71–78.
73. Malicki J, Neuhauss SC, Schier AF, et al. Mutations affecting development of the zebrafish retina. *Development.* 1996;123:263–273.